This is the peer-reviewed, final accepted version for American Mineralogist, published by the Mineralogical Society of America.
The published version is subject to change. Cite as Authors (Year) Title. American Mineralogist, in press.
DOI: https://doi.org/10.2138/am-2022-8429. http://www.minsocam.org/

Revision 1

High-temperature phase relations of hydrous aluminosilicates at 22 GPa in the $AlOOH$-$AlSiO_3OH$ system

Goru Takaichi[1]*, Masayuki Nishi[1,2]*, Youmo Zhou[1,3], Shinichi Machida[4], Ginga Kitahara[5], Akira Yoshiasa[5], and Tetsuo Irifune[1,6]

[1] Geodynamics Research Center, Ehime University, Matsuyama, Ehime 790-8577, Japan

[2] Department of Earth and Space Science, Graduate School of Science, Osaka University, Toyonaka, Osaka 560-0043, Japan

[3] Department of Earth and Planetary Science, Graduate School of Science, Kyusyu University, Fukuoka, Fukuoka 819-0395, Japan

[4] CROSS, Neutron Science and Technology Center, Ibaraki 319-1106, Japan

[5] Graduate School of Science and Technology, Kumamoto University, Kumamoto 860-8555, Japan

[6] Earth-Life Science Institute, Tokyo Institute of Technology, Tokyo 152-8550, Japan

*Corresponding authors

Goru Takaichi,

E-mail: takaichi@sci.ehime-u.ac.jp

Masayuki Nishi,

E-mail: nishimasa@ess.sci.osaka-u.ac.jp

This is the peer-reviewed, final accepted version for American Mineralogist, published by the Mineralogical Society of America.
The published version is subject to change. Cite as Authors (Year) Title. American Mineralogist, in press.
DOI: https://doi.org/10.2138/am-2022-8429. http://www.minsocam.org/

ABSTRACT

The stabilities of the minerals that can hold water are important for understanding the water behavior in the Earth's deep interior. Recent experimental studies have shown that the incorporation of aluminum enhances the thermal stabilities of hydrous minerals significantly. In this study, the phase relations of hydrous aluminosilicates in the AlOOH-$AlSiO_3OH$ system were investigated at 22 GPa and 1400–2275 K using a multi-anvil apparatus. Based on the X-ray diffraction measurements and composition analysis of the recovered samples, we found that the $AlSiO_4H$ phase Egg forms a solid solution with δ-AlOOH above 1500 K. Additionally, at temperatures above 1800 K, two unknown hydrous aluminosilicates with compositions $Al_{2.03}Si_{0.97}O_6H_{2.03}$ and $Al_{2.11}Si_{0.88}O_6H_{2.11}$ appeared, depending on the bulk composition of the starting materials. Both the phases can host large amount of water at least up to 2275 K, exceeding the typical mantle geotherm. The extreme thermal stability of hydrous aluminosilicates suggests that deep-subducted crustal rocks could be a possible reservoir of water in the mantle transition zone and the uppermost lower mantle.

This is the peer-reviewed, final accepted version for American Mineralogist, published by the Mineralogical Society of America.
The published version is subject to change. Cite as Authors (Year) Title. American Mineralogist, in press.
DOI: https://doi.org/10.2138/am-2022-8429. http://www.minsocam.org/

INTRODUCTION

Recent experimental studies have suggested that mantle materials can hold an amount of water exceeding that stored in the ocean (e.g., Fu et al. 2019; Inoue et al. 1995; Litasov et al. 2003). However, the actual storage capacity and the detailed distribution of water remain unclear. The mantle transition zone can be a major water reservoir because ringwoodite and wadsleyite, the dominant minerals, can retain water up to 2–3 wt% in their crystal structures (e.g., Inoue et al. 1995; Kohlstedt et al. 1996). The discovery of hydrous ringwoodite in diamond implies that the transition zone is wet, at least locally (Pearson et al. 2014). In contrast, water solubility in the lower-mantle minerals, such as bridgmanite and magnesiowüstite, is considerably low (e.g., Liu et al., 2021; Fu et al., 2019; N. Bolfan-Casanova, et al., 2002). Because of the contrast in water capacity, the mantle convection to the lower mantle across the transition zone causes a release of water, resulting in dehydration melting, producing seismic low-velocity anomalies (e.g., Liu et al. 2018; Nakajima et al. 2019; Schmandt et al. 2014). Thus, the stabilities of the minerals that can hold water, are important for understanding the water behavior in the Earth's deep interior.

The storage capacity of water in the cold plate subducted into the mantle is much larger than that of the surrounding mantle because dense hydrous magnesium silicates (DHMSs) can be stabilized there (e.g., Nishi et al. 2014; Ohtani et al. 2014). Although these hydrous minerals may deliver water to the mantle, most of the hydrous minerals are stable only in extremely cold regions in the subducted plate. Furthermore, recent experimental studies have showed that the incorporation of aluminum enhances the

thermal stabilities of DHMSs significantly (e.g., Panero and Caracas 2017; Xu et al. 2021). For instance, the aluminum endmember of $Al_2SiO_6H_2$ phase D can endure without dehydration within mafic rocks at temperatures at least up to 2000 °C at 26 GPa, suggesting the potential of hydrous phase as the host for water under the typical mantle geotherm (Pamato et al. 2015). This finding suggests that the water released from DHMSs in ultramafic rocks could be re-trapped in aluminous hydrous minerals in the Al-rich mafic crustal section in the deep mantle.

Many high-pressure hydrous phases have been found in the Al_2O_3-SiO_2-H_2O ternary system. Among them, δ-AlOOH (Suzuki et al. 2000), phase Egg (Eggleton et al. 1978), and aluminous phase D (Pamato et al. 2015) are stable under the pressure and temperature conditions corresponding to the mantle transition zone and the uppermost lower mantle (Abe et al. 2018; Fukuyama et al. 2017). These phases are the key minerals for understanding the Earth's deep water cycle because they have been found as inclusions in superdeep diamonds (Kaminsky 2017; Wirth et al. 2007). In this study, we investigated the high temperature stability of hydrous aluminosilicates at 22 GPa using a multi-anvil apparatus. We found that new hydrous aluminosilicates are stabilized at extreme high temperatures exceeding the typical mantle geotherm.

METHODS

The high-pressure and high-temperature experiments were conducted using a 2000-ton Kawai-type multi-anvil apparatus (Orange 2000) at the Geodynamics Research Center, Ehime University. The pressure and temperature conditions were 22 GPa and 1400–2275 K. Under these conditions, δ-AlOOH, phase Egg, and aluminous phase D are stable, according to the previous studies (Fukuyama et al. 2017; Pamato et al. 2015).

Chemical compositions of the starting materials (Table 1) vary within the AlOOH-$AlSiO_3OH$ binary system. We prepared the starting materials by mixing SiO_2 quartz (Sigma-Aldrich Japan CO., LTD.), Al_2O_3 corundum (KANTO CHEMICAL CO., INC.), $Al(OH)_3$ gibbsite (FUJIFILM WAKO PURE CHEMICAL CO., LTD.), and AlOOH boehmite (TAIMEI CHEMICALS CO., LTD.). For simplicity, we use the Al/(Al+Si) ratios to name the distinct starting materials. For examples, Al0.5 refers to $AlSiO_3OH$, and Al0.67 refers to $Al_2SiO_6H_2$.

Tungsten carbide cubes with the truncated edge length of 4 mm were used as the second-stage anvils. The sample assembly was composed of a semi-sintered Co-doped MgO pressure medium, MgO spacers, a $LaCrO_3$ heater, and two platinum sample capsules. The temperature was monitored using a W3%Re-W25%Re thermocouple. Details of the pressure calibration can be found in the supplementary materials of a previous report (Zhou et al. 2018). In each run, the samples were first pressurized at room temperature, and subsequently heated to the desired temperatures at a heating rate of ~100 K/min. The

heating retention time was 5–180 min. The samples were quenched to the room temperature and were recovered after decompression. The experimental conditions and results are summarized in Table 1.

The recovered samples were mounted in epoxy resin and were polished with diamond paste. A micro-area X-ray diffractometer (Rigaku MicroMax-007HF) and micro-Raman spectrometer (Jasco NRS-5100gr) were used for phase identification. CuKα radiation with a rotating anode was used at 40 kV and 30 mA. A field-emission electron microscope (FESEM, JEOL JSM7000F) equipped with an energy-dispersive X-ray spectrometer (EDS, Oxford Instruments X-Max^N) was used to observe the sample textures and determine the chemical compositions of the observed phases. The chemical analyses were performed on at least ten different grains for the same phase. The standard materials of quantification were forsterite for Si and corundum for Al. Table 2 shows the chemical compositions of the measured phases.

The weight of H_2O contained in the hydrous phases was roughly estimated from the weight loss in the EDS analysis total, based on the same procedure as that specified by Nishi et al. (2014). The ideal weight defect of a hydrous mineral in the EDS analysis is expressed by the proportion of the atomic weight of H_2O in the overall atomic weight of the hydrous mineral. Therefore, the total weight of a hydrous mineral equals 100% minus the relative weight of H_2O. For example, the ideal total weight of aluminous phase D ($Al_2SiO_6H_2$) is ~90 wt%.

RESURTS AND DISCUSSION

Formation of δ-AlOOH–phase Egg solid solutions

At relatively low temperatures of 1400 K and 1475 K, the back-scattered electron images and the compositional analyses of the recovered samples show the presence of δ-AlOOH and phase Egg in the bulk compositions of Al0.67–0.73 (Figure 1a; Table 1). This phase assemblage is confirmed by the corresponding XRD patterns (Figure 2a) and is consistent with the results reported by Abe et al. (2018). Phase Egg obtained in these runs has the stoichiometric end-member composition $AlSiO_3OH$, while δ-AlOOH contains some amounts of Si (Table 2).

The same phase assemblage was obtained from Al0.67–0.68 at higher temperatures of 1675 K and 1800 K. However, the Al content in the phase Egg increases from Al/(Al+Si) = 0.5 for $AlSiO_3OH$, which suggests the formation of solid solutions between δ-AlOOH and phase Egg. Notably, the solid–solution reactions occur on phase Egg at temperatures above ~1500 K, while they are initiated on δ-AlOOH at lower temperatures. Additionally, we found that the Si-bearing δ-AlOOH survives up to 1800 K, which exceeds the dehydration temperature of δ-AlOOH, ~1473 K, determined by Yoshino et al. (2019). Therefore, Si substitution in δ-AlOOH that occurred in this study may increase the dehydration temperature.

To obtain the structural information of the Al-rich phase Egg, we attempted to synthesize a single-phase product of Al-rich phase Egg with a chemical composition of $Al_{1.18}Si_{0.82}O_4H_{1.18}$ at 2000 K (Figure

1b and Table 2). Although all the XRD peaks of this Al-rich phase Egg are indexed by the crystal structure of phase Egg (Figure 2b), some changes in the unit cell parameters owing to the Al-rich composition are recognized. The obtained unit cell parameters are a = 7.207(2) Å, b = 4.321(1) Å, c = 7.017(2) Å, beta = 98.194(9)°, and V = 216.3(2) $Å^3$, and they are slightly different from those of the endmember phase Egg (a = 7.14409(2) Å, b = 4.33462(1) Å, c = 6.95255(2) Å, beta = 98.396(1)°, and V = 212.99(1) $Å^3$) (Schmidt et al. 1998), as shown in Figure S1. Increases in the *a/b* axial ratio and cell volume as a function of Al content were observed in phase Egg, which is explained by the fact that Al has a slightly larger ionic radius than Si. The increase in cell volume from the Al + H substitution for Si sites was observed in stishovite by Smith et al. (2015).

Occurrence of unknown hydrous phases at higher temperatures

In the sample Al0.68 obtained at 1800 K, we observed not only the assemblage of δ-AlOOH and phase Egg at the low-temperature (LT) part (far from the thermocouple) of the capsule, but also a different phase assemblage at the high-temperature (HT) part (close to the thermocouple) of the capsule (Figure 1c). This phase segregation is caused by the thermal gradient. The temperature difference may reach 125 K because the compositions of δ-AlOOH and phase Egg in the LT part are similar to those observed at 1675 K (Table 1). This different phase assemblage contains Al-rich phase Egg with a chemical composition of $Al_{1.15}Si_{0.85}O_4H_{1.15}$ (Al0.58) and an Al-richer unknown phase with a chemical composition of

$Al_{2.07}Si_{0.93}O_6H_{2.07}$ (Al0.67; hereafter referred to as unknown phase I) (Figure 1d and Table 2). The XRD peaks of unknown phase I cannot be indexed to phase Egg or the other hydrous aluminosilicates, such as aluminous phase D (Pamato et al. 2015) and topaz OH-II (Kanzaki, 2010). Furthermore, at the same temperature of 1800 K, we obtained another unknown hydrous phase (hereafter referred to as unknown phase II) in the sample Al0.71, and this phase shows a slightly higher Al/(A+Si) ratio (0.70) (Table 2), in comparison to unknown phase I.

In the experiments performed at temperatures of 1900–2275 K, the Al-rich phase Egg, unknown phase I, and unknown phase II were repeatedly synthesized from the starting materials with different Al/(Al+Si) ratios (Table 1). The products depend strongly on the bulk compositions of the starting materials. The chemical composition of Al-rich phase Egg changed, while the chemical compositions of both the unknown phases did not change drastically with temperature (Table 2), suggesting that the two unknown phases are the chemically invariable intermediate phases in the $AlOOH$-$AlSiO_3OH$ binary system. Unknown phase I and II show the Al/(Al+Si) ratios of ~0.67 and ~0.71, respectively. When the Al/(Al+Si) ratio is above ~0.71, in addition to the formation of unknown phase II, the additional Al component transformed into corundum and fluid (Table 1).

Although the XRD patterns of the Al-rich phase Egg, unknown phase I, and unknown phase II appear similar (Figure 2b–d), it is difficult to clarify their crystal structures at this moment. The *d*-values and intensities of peaks of the two unknown phases are presented in Table S1. Indeed, it is not certain

whether the three phases have the same crystal structure or whether the two unknown phases have the same crystal structure, given the similar chemical compositions. However, as shown in Figure 1d and Figure 3, unknown phase I can coexist with Al-rich phase Egg and unknown phase II. Therefore, these three phases should have different crystal structures. Figure S3 shows the Raman spectra of the unknown phases and the broad peak at 2000–3700 cm^{-1}, which indicates a typical OH stretching mode.

Substitution mechanisms for Al-rich phase Egg and the two unknown phases

Figure 4 summarizes the total weights of the hydrous phases obtained in our experiments as a function of the Al/(Al+Si) ratio. These total weights are obviously less than 100% owing to the weight loss of H_2O in the EDS analyses. In Figure 4, we also show the ideal weight totals of SiO_2 stishovite, $AlSiO_3OH$ phase Egg, $Al_2SiO_6H_2$ aluminous phase D, and δ-AlOOH for reference. Based on the relationships between the chemical compositions of these phases, it is intuitive that the substitution mechanism in the AlOOH-$AlSiO_3OH$ binary system is $Al^{3+} + H^+ = Si^{4+}$. This mechanism defines the same atomic number of Al and H in the chemical formulas of the hydrous phases. Therefore, the weight totals of these phases change linearly with the Al/(Al+Si) ratio. In comparison with the ideal cases, the weight totals of the hydrous phases obtained in our experiments also change linearly with the Al/(Al+Si) ratio, and the slope is close to that in the ideal cases that is strongly supportive of the substitution mechanism of $Al^{3+} + H^+ = Si^{4+}$ for the formation of Al-rich phase Egg and the two unknown phases. The accordance

176 between our data and the ideal cases suggests that the water contents of hydrous minerals can be estimated
177 with appropriate accuracy based on the weight loss of water in the chemical analysis.
178
179 **Phase relations of the AlOOH-$AlSiO_3OH$ binary system at 22 GPa**
180 Figure 5 shows the phase relations of the AlOOH-$AlSiO_3OH$ binary system at 22 GPa that are
181 determined based on our experimental results (Table 1 and Table 2). At temperatures below 1800 K, phase
182 Egg and δ-AlOOH form solid solutions, and these two phases coexist. This two-phase coexistence was
183 reported in the previous studies (Fukuyama et al. 2017; Sano et al. 2004), while the previous studies did
184 not observe the occurrence of Al-rich phase Egg owing to the lower experimental temperatures. Above
185 1800 K, phase Egg is still stable, and the solubility of AlOOH components further increases with
186 temperature, while δ-AlOOH disappears. Instead, two unknown phases can be formed, and they have
187 considerably similar Al/(Al+Si) ratios that are much higher than that of the Al-rich phase Egg. With
188 temperature change, the chemical composition of Al-rich phase Egg changed, while those of both the
189 unknown phases did not change drastically. Therefore, they are expected to be the chemically invariable
190 intermediate phases in the binary system, and they result from the isothermal reactions between phase Egg
191 and δ-AlOOH at temperatures above 1800 K. Relative to unknown phase I, unknown phase II is slightly
192 richer in Al. For further Al-rich chemical compositions relative to that of unknown phase II, in addition to
193 the formation of unknown phase II, the additional components transform into corundum and fluid.

Fukuyama et al. (2017) reported that phase Egg decomposes into aluminous phase D, corundum, and stishovite at 22 GPa and 1773 K. In contrast, our experimental results show that phase Egg can survive at 22 GPa up to 2000 K and contain more Al than $AlSiO_3OH$ at such high temperatures. The previous study might have misidentified the Al-rich phase Egg as aluminous phase D because of the similarities between these two phases in the Raman spectra (Figure S2) and chemical compositions. Our results are comparable to those of the previous studies (Abe et al. 2018; Pamato et al. 2015) that suggest that phase Egg is stable at the uppermost lower mantle. In addition, we found two unknown hydrous phases that are not identical to aluminous phase D, although the chemical compositions are considerably similar. Further experimental studies covering a much wider pressure and temperature range are required to understand the phase relations of the Al_2O_3-SiO_2-H_2O system.

IMPLICATIONS

From our results and those of the earlier studies (Abe et al. 2018; Liu et al. 2019; Ono, 1999), it is confirmed that phase Egg and δ-AlOOH are stable in the hydrated sediment and basalt rocks under the pressures of the mantle transition zone and the top of the lower mantle. However, the hydroxides that appear in the sediment rocks in the upper mantle, such as AlOOH diaspore and FeOOH goethite, are improbable candidates for transporting the surface water to the deep mantle because they generally breakdown in the early stage of subduction (Yoshino et al., 2019). Therefore, the phase Egg found in the

ultradeep diamond might suggest that the sediment captures the water released from the underlying ultramafic rocks after the deep plate subduction to the mantle transition zone or the lower mantle (Nishi et al. 2019; Pamato et al. 2015). Such rehydration may occur in the lower mantle rather than the mantle transition zone where the ringwoodite in ultramafic rocks can host a large amount of water in the mantle transition zone. The rehydration may also be caused by the other minerals in the subducted crustal rocks, such as stishovite and CaPv, which are able to retain water at high pressures as well (Lin et al., 2020; Németh et al. 2017).

Considering the thermal stability of hydrous aluminosilicates under pressures of the bottom of the mantle transition zone, the hydrated sediments retain water even after the plate stagnation at a depth of ~660 km. The temperature increase during the stagnation may change the composition and the structure of hydrous phases, as shown in this study. When the hydrated sediments move outside the stability field of the hydrous aluminosilicates through the mantle convection, the released water may cause dehydration melting and produce seismic low-velocity anomalies (e.g., Liu et al. 2018; Nakajima et al. 2019; Schmandt et al. 2014). However, their phase relations at around the mantle transition zone and the uppermost of the lower mantle have not been fully understood yet. Further studies based on the precise experimental studies on the multicomponent system (including Mg and Fe) would provide a better understanding of the water behavior in the deep mantle.

ACKNOWLEDGMENTS

The authors declare no competing financial interests. We thank Prof. A. Suzuki and Prof. T. Inoue for the constructive discussion and comments. This work was supported by MEXT/JSPS KAKENHI (grant number 19H01994 to M.N. and grant number JP15H05829 to M.N. and T.I.)

REFERENCES

Abe, R., Shibazaki, Y., Ozawa, S., Ohira, I., Tobe, H., and Suzuki, A. (2018) In situ X-ray diffraction studies of hydrous aluminosilicate at high pressure and temperature. Journal of Mineralogical and Petrological Sciences, 113, 106–111. https://doi.org/10.2465/jmps.170714

Bolfan-Casanova, N., Mackwell, S., Keppler, H., McCammon, C., & Rubie, D. C. (2002). Pressure dependence of H solubility in magnesiowüstite up to 25 GPa: Implications for the storage of water in the Earth's lower mantle. Geophysical Research Letters, 29(10), 89-1. https://doi.org/10.1029/2001GL014457

Eggleton, R.A., Boland, J.N., and Ringwood, A.E. (1978) High pressure synthesis of a new aluminium silicate: $Al_5Si_5O_{17}$ (OH). Geochemical Journal, 12, 191–194. https://doi.org/10.2343/geochemj.12.191

Fu, S., Yang, J., Karato, S.I., Vasiliev, A., Presniakov, M.Y., Gavrilliuk, A.G., Ivanova, A.G., Hauri, E.H., Okuchi, T., Purevjav, N., and Lin, J.F. (2019) Water Concentration in Single-Crystal (Al,Fe)-Bearing Bridgmanite Grown From the Hydrous Melt: Implications for Dehydration Melting at the Topmost Lower Mantle. Geophysical Research Letters, 46, 10346–10357. https://doi.org/10.1029/2019GL084630

Fukuyama, K., Ohtani, E., Shibazaki, Y., Kagi, H., and Suzuki, A. (2017) Stability field of phase Egg, $AlSiO_3OH$ at high pressure and high temperature: possible water reservoir in mantle transition zone. Journal of Mineralogical and Petrological Sciences, 112, 31–35. https://doi.org/10.2465/jmps.160719e

Inoue, T., Yurimoto, H., and Kudoh, Y. (1995) Hydrous modified spinel, $Mg_{1.75}SiH_{0.5}O_4$: A new water reservoir in the mantle transition region. Geophysical Research Letters, 22, 117–120. https://doi.org/10.1029/94GL02965

Kaminsky, F.V. (2017) Mafic lower-mantle mineral association. Springer Geology, p. 161–203.

https://doi.org/10.1007/978-3-319-55684-0_5

Kanzaki, M. (2010) Crystal structure of a new high-pressure polymorph of topaz-OH. American Mineralogist, 95, 1349–1352. https://doi.org/10.2138/am.2010.3555

Kohlstedt, D.L., Keppler, H., and Rubie, D.C. (1996) Solubility of water in the α, β and γ phases of $(Mg,Fe)_2SiO_4$. Contributions to Mineralogy and Petrology, 123, 345–357. https://doi.org/10.1007/s004100050161

Litasov, K., Ohtani, E., Langenhorst, F., Yurimoto, H., Kubo, T., and Kondo, T. (2003) Water solubility in Mg-perovskites and water storage capacity in the lower mantle. Earth and Planetary Science Letters, 211, 189–203. https://doi.org/10.1016/S0012-821X(03)00200-0

Liu, Z., Park, J., and Karato, S.-i. (2018) Seismic evidence for water transport out of the mantle transition zone beneath the European Alps. Earth and Planetary Science Letters, 482, 93–104. https://doi.org/10.1016/j.epsl.2017.10.054

Liu, Z., Fei, H., Chen, L., McCammon, C., Wang, L., Liu, R., ... & Katsura, T. (2021). Bridgmanite is nearly dry at the top of the lower mantle. Earth and Planetary Science Letters, 570, 117088. https://doi.org/10.1016/j.epsl.2021.117088

Liu, X., Matsukage, K.N., Nishihara, Y., Suzuki, T., and Takahashi, E. (2019) Stability of the hydrous phases of Al-rich phase D and Al-rich phase H in deep subducted oceanic crust. American Mineralogist, 104, 64–72. https://doi.org/10.2138/am-2019-6559

Lin, Y., Hu, Q., Meng, Y., Walter, M., & Mao, H. K. (2020) Evidence for the stability of ultrahydrous stishovite in Earth's lower mantle. Proceedings of the National Academy of Sciences, 117(1), 184-189. https://doi.org/10.1073/pnas.1914295117

Nakajima, A., Sakamaki, T., Kawazoe, T., and Suzuki, A. (2019) Hydrous magnesium-rich magma genesis at the top of the lower mantle. Scientific Reports, 9(1), 7420. https://doi.org/10.1038/s41598-019-43949-2

Németh, P., Leinenweber, K., Ohfuji, H., Groy, T., Domanik, K.J., Kovács, I.J., Kovács, J.S., Buseck, P.R. (2017) Water-bearing, high-pressure Ca-silicates. Earth and Planetary Science Letters, 469, 148-155. http://doi.org/10.2138/am-2022-8009

Nishi, M., Irifune, T., Tsuchiya, J., Tange, Y., Nishihara, Y., Fujino, K., and Higo, Y. (2014) Stability of hydrous silicate at high pressures and water transport to the deep lower mantle. Nature Geoscience, 7, 224–227. https://doi.org/10.1038/ngeo2074

Nishi, M., Tsuchiya, J., Kuwayama, Y., Arimoto, T., Tange, Y., Higo, Y., Hatakeyama, T., and Irifune, T. (2019) Solid Solution and Compression Behavior of Hydroxides in the Lower Mantle. Journal of Geophysical Research: Solid Earth, 124, 10231–10239. https://doi.org/10.1029/2019JB018146

Ohtani, E., Amaike, Y., Kamada, S., Sakamaki, T., and Hirao, N. (2014) Stability of hydrous phase H MgSiO4H2 under lower mantle conditions. Geophysical Research Letters, 41, 8283–8287.

https://doi.org/10.1002/2014GL061690

Ono, S. (1999) High temperature stability limit of phase egg, AlSiO3(OH). Contributions to Mineralogy and Petrology, 137, 83–89. https://doi.org/10.1007/s004100050583

Pamato, M.G., Myhill, R., Boffa Ballaran, T., Frost, D.J., Heidelbach, F., and Miyajima, N. (2015) Lower-mantle water reservoir implied by the extreme stability of a hydrous aluminosilicate. Nature Geoscience, 8, 75–79. https://doi.org/10.1038/ngeo2306

Panero, W.R., and Caracas, R. (2017) Stability of phase H in the $MgSiO_4H_2$-AlOOH-SiO_2 system. Earth and Planetary Science Letters, 463, 171–177. https://doi.org/10.1016/J.EPSL.2017.01.033

Pearson, D.G., Brenker, F.E., Nestola, F., McNeill, J., Nasdala, L., Hutchison, M.T., Matveev, S., Mather, K., Silversmit, G., Schmitz, S., Vekemans, B., and Vincze, L. (2014) Hydrous mantle transition zone indicated by ringwoodite included within diamond. Nature, 507, 221–224. https://doi.org/10.1038/nature13080

Sano, A., Ohtani, E., Kubo, T., and Funakoshi, K.-i. (2004) In situ X-ray observation of decomposition of hydrous aluminum silicate AlSiO3OH and aluminum oxide hydroxide d-AlOOH at high pressure and temperature. Journal of Physics and Chemistry of Solids, 65, 1547–1554. https://doi.org/10.1016/j.jpcs.2003.12.015

Schmandt, B., Jacobsen, S.D., Becker, T.W., Liu, Z., and Dueker, K.G. (2014) Dehydration melting at the top of the lower mantle. Science, 344, 1265–1268. https://doi.org/10.1126/science.1253358

Schmidt, M.W., Finger, L.W., Angel, R.J., and Dinnebier, R.E. (1998) Synthesis, crystal structure, and phase relations of AlSiO3OH, a high-pressure hydrous phase. American Mineralogist, 83, 881–888. https://doi.org/10.2138/am-1998-7-820

Smith, J.R., Swope, R.J., and Pawley A.R. (1995) H in rutile-type compounds: II. Crystal chemistry of Al-substitution in H-bearing stishovite. American mineralogist, 80, 454-456. https://doi.org/10.2138/am-1995-5-605

Suzuki, A., Ohtani, E., and Kamada, T. (2000) A new hydrous phase δ-Al00H synthesized at 21 GPa and 1000 °C. Physics and Chemistry of Minerals, 27, 689–693. https://doi.org/10.1007/s002690000120

Wirth, R., Vollmer, C., Brenker, F., Matsyuk, S., and Kaminsky, F. (2007) Inclusions of nanocrystalline hydrous aluminium silicate “Phase Egg” in superdeep diamonds from Juina (Mato Grosso State, Brazil). Earth and Planetary Science Letters, 259, 384–399. https://doi.org/10.1016/j.epsl.2007.04.041

Xu, C., Inoue, T., Kakizawa, S., Noda, M., and Gao, J. (2021) Effect of Al on the stability of dense hydrous magnesium silicate phases to the uppermost lower mantle: implications for water transportation into the deep mantle. Physics and Chemistry of Minerals, 48. https://doi.org/10.1007/s00269-021-01156-4

329 Yoshino, T., Baker, E., & Duffey, K. (2019). Fate of water in subducted hydrous sediments deduced from
330 stability fields of FeOOH and AlOOH up to 20 GPa. Physics of the Earth and Planetary Interiors,
331 294, 106295. https://doi.org/10.1016/j.pepi.2019.106295
332 Zhou, Y., Irifune, T., Ohfuji, H., and Kuribayashi, T. (2018) New High-Pressure Forms of Al_2SiO_5.
333 Geophysical Research Letters, 45, 8167–8172. https://doi.org/10.1029/2018GL078960

334 LIST OF FIGURE CAPTIONS

335 **Figure 1.** Back-scattered electron images showing the textures of the recovered samples. (a) Recovered
336 sample from 1400 K (Al0.68, OS3663). (b) Recovered sample from 2000 K (Al0.60, OS3558). A single
337 phase of Al-rich phase Egg with a composition of $Al_{1.18}Si_{0.82}O_4H_{1.18}$ was obtained. (c) Recovered sample
338 from 1800 K (Al0.68, OS3668). Discontinuous change in the phase assemblage due to thermal gradient
339 was observed. (d) Large magnification of the higher temperature side (HT) of (c). Abbreviations: Egg,
340 Phase Egg; δ, δ-AlOOH; PhI, unknown phase I; PhII unknown phase II.
341
342
343 **Figure 2.** Selected XRD patterns of the run products. (a) Coexistence of the phase Egg and δ-AlOOH
344 (Al0.68, OS3663). (b) Al-rich phase Egg (Al0.60, OS3558). (c) Unknown phase I (Al0.67, OS3582). (d)
345 Unknown phase II (Al0.71, OS3582).
346
347 **Figure 3.** BSE image and elemental mapping images for Al and Si of the recovered sample from 2000 K
348 (OS3558). Coexistence of PhI and PhII is observed.
349
350 **Figure 4.** Weight deficit attributed to the amount of H_2O in the analyzed total of the recovered minerals
351 as a function of the Al number. Gray symbols show the ideal values calculated based on the stoichiometric
352 composition of the hydrous minerals.
353

354 **Figure 5.** Phase relations in the $AlSiO_3OH$-AlOOH system at 22 GPa. The blue squares represent the
355 compositions of phase egg and coexisting δ-AlOOH. The orange circles represent the compositions of
356 phase egg and coexisting unknown phase I. The green rhombuses represent the compositions of unknown
357 phase I and coexisting unknown phase II. The red and blue triangles represent the composition of single
358 phase of unknown phase I and unknown phase II, respectively. We assumed 1750 K and 1850 K
359 corresponding to the low-temperature regions of OS3668 and OS3676, respectively. The phase relations
360 in the Al numbers above 0.73 and the temperatures above 2000 K are unknown due to the lack of data on
361 the coexisting relationship of the phases. Abbreviations: Egg, phase Egg; δ, δ-AlOOH; Al-Egg, Al-rich
362 phase Egg; PhI, unknown phase I; PhII, unknown phase II; Cor, corundum; F, fluid.
363

This is the peer-reviewed, final accepted version for American Mineralogist, published by the Mineralogical Society of America.
The published version is subject to change. Cite as Authors (Year) Title. American Mineralogist, in press.
DOI: https://doi.org/10.2138/am-2022-8429. http://www.minsocam.org/

364 TABLES

365 Table 1. Experimental conditions and run products

Run No.	Temperature (K)	Duration (min)	Starting material(a)	Phase assemblages(b)
OS3663	1400	180	$Al_{2.03}Si_{0.97}O_6H_{2.03}$ (0.68)	Egg (0.50), δ (0.90), St[c]
			$Al_{2.12}Si_{0.88}O_6H_{2.12}$ (0.71)	Egg (0.50), δ (0.91)
OD1906	1475	120	$Al_{2.00}Si_{1.00}O_6H_{2.00}$ (0.67)	Egg (0.50), δ (0.93)
OD1899	1675	90	$Al_{2.00}Si_{1.00}O_6H_{2.00}$ (0.67)	Al-Egg (0.55), δ (0.88)
OS3668	1800	30	$Al_{2.03}Si_{0.97}O_6H_{2.03}$ (0.68)	HT: Al-Egg (0.58), PhI (0.69)
				LT: Al-Egg (0.55), δ (0.87)
			$Al_{2.12}Si_{0.88}O_6H_{2.12}$ (0.71)	PhII (0.70)
OS3676	1900	30	$Al_{1.97}Si_{1.03}O_6H_{1.97}$ (0.66)	HT: PhI (0.65)
				LT: Al-Egg (0.59), PhI (0.67)
			$Al_{2.25}Si_{0.75}O_6H_{2.25}$ (0.75)	PhII (0.74), Cor[c], Fluid[c], PhII (0.71)[c]
OS3558	2000	20	$Al_{2.09}Si_{0.91}O_6H_{2.09}$ (0.70)	PhI (0.67), PhII (0.71)
			$Al_{1.20}Si_{0.80}O_4H_{1.20}$ (0.60)	Egg (0.59)
OS3582	2000	5	$Al_{2.00}Si_{1.00}O_6H_{2.00}$ (0.67)	PhI (0.68)
			$Al_{2.14}Si_{0.86}O_6H_{2.14}$ (0.71)	PhII (0.71)
OS3683	2000	20	$Al_{1.89}Si_{1.11}O_6H_{1.89}$ (0.63)	Egg (0.60), PhI (0.68)
			$Al_{1.09}Si_{0.91}O_6H_{1.09}$ (0.55)	Egg (0.54)
OD1893	2275	15	$Al_{2.00}Si_{1.00}O_6H_{2.00}$ (0.67)	PhI (0.67)
			$Al_{1.85}Si_{0.71}O_6H_{3.62}$ (0.72)	PhII (0.71), Fluid[c]

366 [a,b,c] indicate Al/(Al+Si) ratio of starting composition, Al/(Al+Si) ratio of the recovered phases and trace

367 amount. Abbreviations: Egg, phase Egg; δ, δ-AlOOH; Cor, corundum; PhI, unknown phase I; PhII,

368 unknown phase II; HT, high-temperature region; LT, low-temperature region.

This is the peer-reviewed, final accepted version for American Mineralogist, published by the Mineralogical Society of America.
The published version is subject to change. Cite as Authors (Year) Title. American Mineralogist, in press.
DOI: https://doi.org/10.2138/am-2022-8429. http://www.minsocam.org/

369 Table 2. Chemical compositions of run products

Run No.	Temperature (K)	Starting material	Products	Al_2O_3 (wt%)	SiO_2 (wt%)	Total (wt%)
OS3663	1400	$Al_{2.03}Si_{0.97}O_6H_{2.03}$	Egg	42.0 (36)	51.4 (38)	93.4 (16)
			δ	75.7 (44)	9.20 (48)	85.0 (20)
		$Al_{2.12}Si_{0.88}O_6H_{2.12}$	Egg	42.6 (13)	51.2 (14)	93.8 (12)
			δ	75.2 (31)	8.31 (25)	83.6 (17)
OD1906	1475	$Al_{2.00}Si_{1.00}O_6H_{2.00}$	Egg	42.8 (4)	50.8 (6)	93.5 (6)
			δ	77.7 (10)	6.4 (11)	83.7 (10)
OD1899	1675	$Al_{2.00}Si_{1.00}O_6H_{2.00}$	Egg	45.4 (6)	45.1 (8)	90.5 (10)
			δ	71.0 (6)	11.7 (4)	83.1 (17)
OS3668	1800	$Al_{2.03}Si_{0.97}O_6H_{2.03}$	Egg (LT)	46.8 (9)	43.2 (8)	90.0 (6)
			δ (LT)	70.3 (13)	13.2 (9)	83.4 (9)
			Egg (HT)	47.5 (7)	41.2 (7)	88.6 (13)
			PhI (HT)	56.3 (9)	30.7 (11)	87.0 (13)
		$Al_{2.12}Si_{0.88}O_6H_{2.12}$	PhII	57.0 (8)	29.3 (6)	86.3 (14)
OS3676	1900	$Al_{1.97}Si_{1.03}O_6H_{1.97}$	PhI (HT)	51.5 (6)	33.1 (5)	84.5 (9)
			Egg (LT)	46.7 (3)	37.5 (3)	84.2 (6)
			PhI (LT)	53.0 (5)	30.9 (4)	84.0 (7)
		$Al_{2.25}Si_{0.75}O_6H_{2.25}$	PhII	58.7 (12)	24.4 (8)	84.0 (14)
OS3558	2000	$Al_{1.20}Si_{0.80}O_4H_{1.20}$	Egg	48.0 (5)	39.5 (4)	87.6 (7)
		$Al_{2.09}Si_{0.91}O_6H_{2.09}$	PhI	56.3 (6)	32.8 (2)	89.1 (6)
			PhII	59.0 (5)	28.5 (3)	87.5 (3)
OS3582	2000	$Al_{2.00}Si_{1.00}O_6H_{2.00}$	PhI	56.7 (5)	32.0 (3)	88.7 (7)
		$Al_{2.14}Si_{0.86}O_6H_{2.14}$	PhII	58.5 (10)	28.9 (9)	87.4 (15)
OS3683	2000	$Al_{1.89}Si_{1.11}O_6H_{1.89}$	Egg	50.1 (5)	37.1 (6)	87.3 (7)
			PhI	54.5 (3)	30.5 (6)	85.4 (5)
		$Al_{1.09}Si_{0.91}O_6H_{1.09}$	Egg	44.2 (5)	44.2 (5)	88.4 (9)
OD1893	2275	$Al_{2.00}Si_{1.00}O_6H_{2.00}$	PhI	56.5(4)	33.2(6)	89.7(9)
		$Al_{1.85}Si_{0.71}O_6H_{3.62}$	PhII	57.5(6)	27.7(2)	85.3(7)

370 Abbreviations: Egg, phase Egg; δ, δ-AlOOH; PhI, unknown phase I; PhII, unknown phase II.

371

This is the peer-reviewed, final accepted version for American Mineralogist, published by the Mineralogical Society of America.
The published version is subject to change. Cite as Authors (Year) Title. American Mineralogist, in press.
DOI: https://doi.org/10.2138/am-2022-8429. http://www.minsocam.org/

372 FIGURES

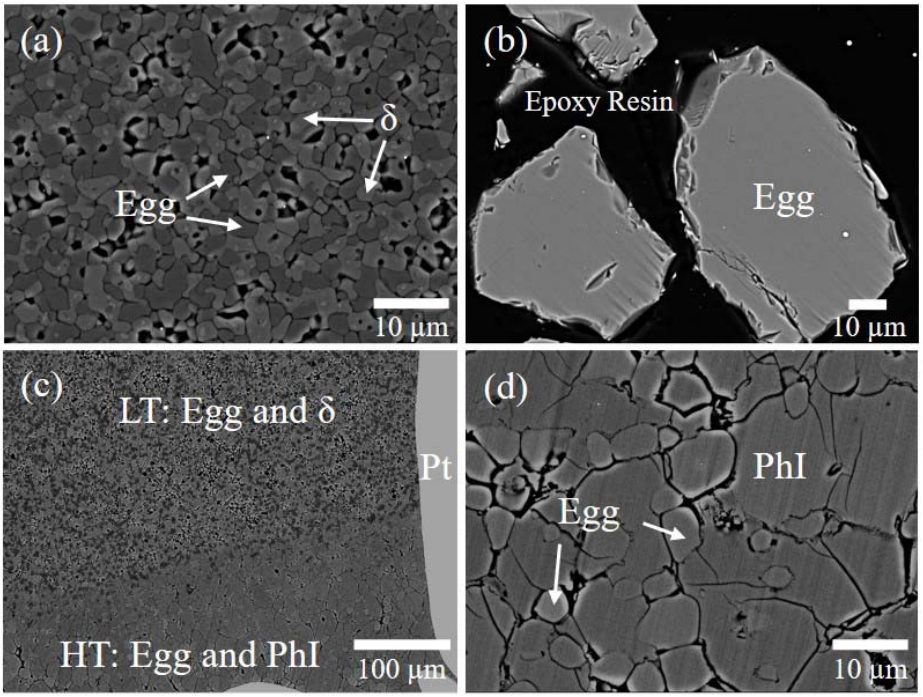

373

374 **Figure 1.** Back-scattered electron images showing the textures of the recovered samples. (a) Recovered
375 sample from 1400 K (Al0.68, OS3663). (b) Recovered sample from 2000 K (Al0.60, OS3558). A single
376 phase of Al-rich phase Egg with a composition of $Al_{1.18}Si_{0.82}O_4H_{1.18}$ was obtained. (c) Recovered sample
377 from 1800 K (Al0.68, OS3668). Discontinuous change in the phase assemblage due to thermal gradient
378 was observed. (d) Large magnification of the higher temperature side (HT) of (c). Abbreviations: Egg,
379 phase Egg; δ, δ-AlOOH; PhI, unknown phase I; PhII unknown phase II.

380

This is the peer-reviewed, final accepted version for American Mineralogist, published by the Mineralogical Society of America.
The published version is subject to change. Cite as Authors (Year) Title. American Mineralogist, in press.
DOI: https://doi.org/10.2138/am-2022-8429. http://www.minsocam.org/

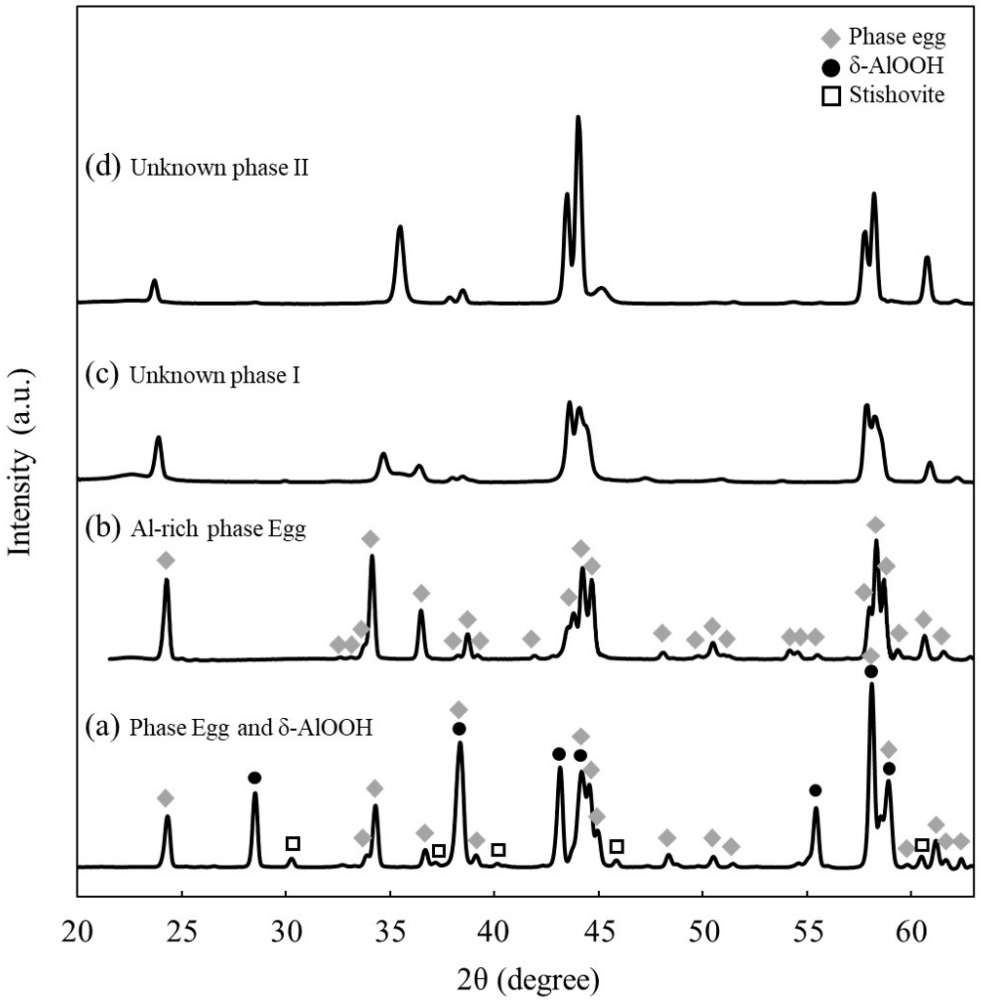

Figure 2. Selected XRD patterns of the run products. (a) Coexistence of the phase Egg and δ-AlOOH (Al0.68, OS3663). (b) Al-rich phase Egg (Al0.60, OS3558). (c) Unknow phase I (Al0.67, OS3582). (d) Unknown phase II (Al0.71, OS3582).

This is the peer-reviewed, final accepted version for American Mineralogist, published by the Mineralogical Society of America.
The published version is subject to change. Cite as Authors (Year) Title. American Mineralogist, in press.
DOI: https://doi.org/10.2138/am-2022-8429. http://www.minsocam.org/

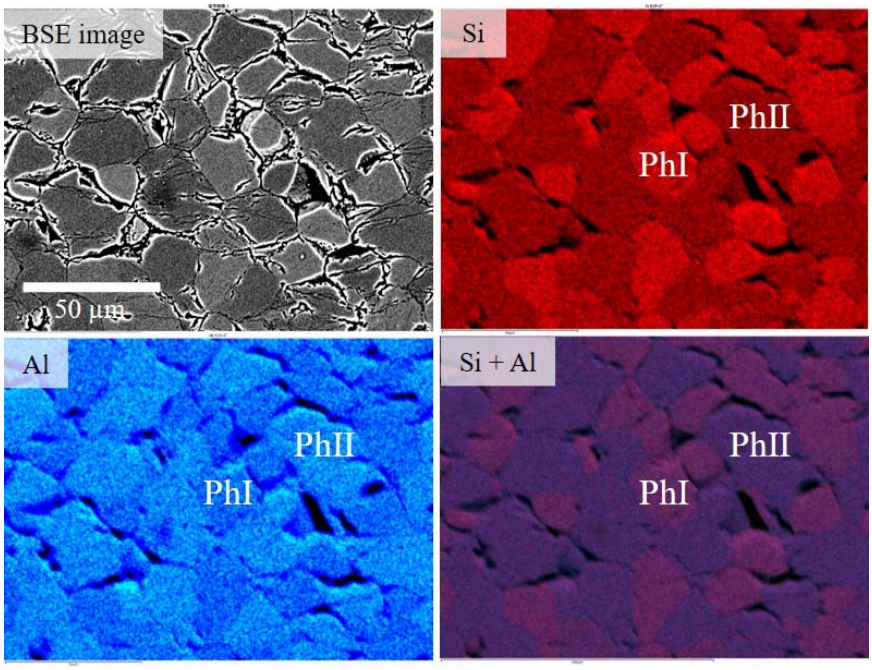

387

388 **Figure 3.** BSE image and elemental mapping images for Al and Si of the recovered sample from 2000 K

389 (OS3558). Coexistence of PhI and PhII is observed.

390

This is the peer-reviewed, final accepted version for American Mineralogist, published by the Mineralogical Society of America.
The published version is subject to change. Cite as Authors (Year) Title. American Mineralogist, in press.
DOI: https://doi.org/10.2138/am-2022-8429. http://www.minsocam.org/

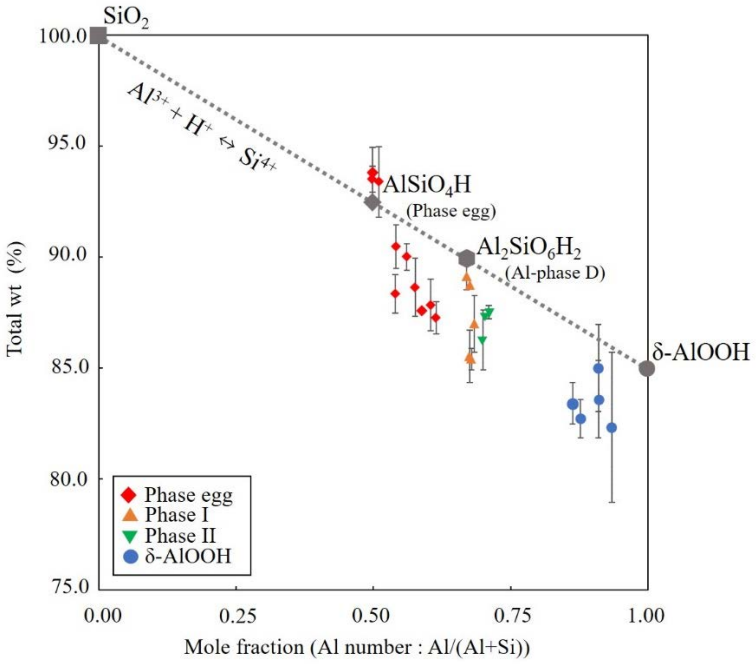

Figure 4. Weight deficit attributed to the amount of H_2O in the analyzed total of the recovered minerals as a function of the Al number. Gray symbols show the ideal values calculated based on the stoichiometric composition of the hydrous minerals. Gray dash line shows the ideal substitution of $Al^{3+} + H^{+} \leftrightarrow Si^{4+}$.

This is the peer-reviewed, final accepted version for American Mineralogist, published by the Mineralogical Society of America.
The published version is subject to change. Cite as Authors (Year) Title. American Mineralogist, in press.
DOI: https://doi.org/10.2138/am-2022-8429. http://www.minsocam.org/

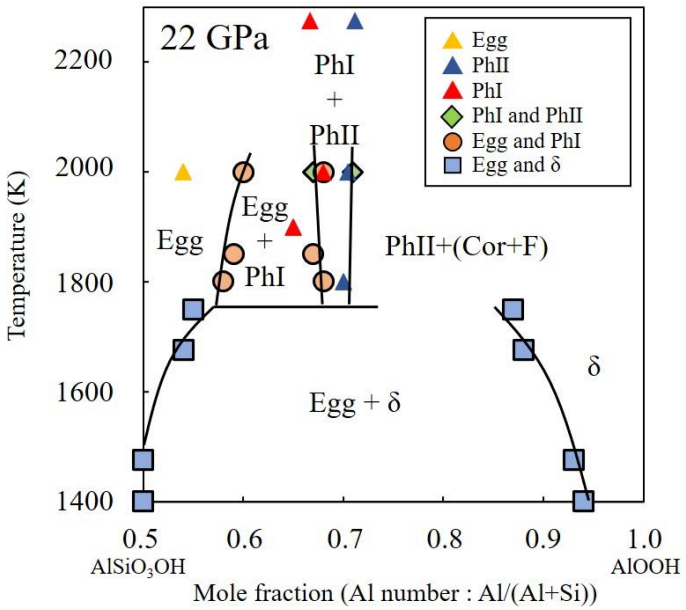

Figure 5. Phase relations in the $AlSiO_3OH$-AlOOH system at 22 GPa. The blue squares represent the compositions of phase Egg and coexisting δ-AlOOH. The orange circles represent the compositions of phase Egg and coexisting unknown phase I. The green rhombuses represent the compositions of unknown phase I and coexisting unknown phase II. The red and blue triangles represent the composition of single phase of unknown phase I and unknown phase II, respectively. We assumed 1750 K and 1850 K corresponding to the low-temperature regions of OS3668 and OS3676, respectively. The phase relations in the Al numbers above 0.73 and the temperatures above 2000 K are unknown due to the lack of data on the coexisting relationship of the phases. Abbreviations: Egg, phase Egg; δ, δ-AlOOH; Al-Egg, Al-rich phase Egg; PhI, unknown phase I; PhII, unknown phase II; Cor, corundum; F, fluid.